IEEE Access
Multidisciplinary | Rapid Review | Open Access Journal

Received April 16, 2022, accepted May 2, 2022, date of publication May 20, 2022, date of current version May 27, 2022.

Digital Object Identifier 10.1109/ACCESS.2022.3176732

Experimental Investigations on Particle Swarm Optimization Based Control Algorithm for Shunt Active Power Filter to Enhance Electric Power Quality

RAVINDER KUMAR[1], HARI OM BANSAL[2], (Senior Member, IEEE), ADITYA R. GAUTAM[2], OM PRAKASH MAHELA[3], (Senior Member, IEEE), AND BASEEM KHAN[4], (Senior Member, IEEE)

[1]Department of Electrical Engineering, Dr. B. R. Ambedkar National Institute of Technology, Jalandhar, Punjab 144027, India
[2]Department of Electrical and Electronics Engineering, Birla Institute of Technology and Science, Pilani, Rajasthan 333031, India
[3]Power System Planning Division, Rajasthan Rajya Vidyut Prasaran Nigam Ltd., Jaipur, Rajasthan 302005, India
[4]Department of Electrical and Computer Engineering, Hawassa University, Awassa 05, Ethiopia

Corresponding author: Baseem Khan (baseem.khan04@ieee.org)

ABSTRACT Quality power is a very important factor for the proper functioning of appliances and can be enhanced using shunt active power filters (SAPF). This work demonstrates the hardware implementation of synchronous reference frame (SRF) theory based SAPF. This paper presents the technique of particle swarm optimization (PSO) to tune the gain values of the SAPF PI controller to control the voltage of the DC-link and enhance its dynamic efficiency. The estimation of gain values of PI controllers using conventional methods does not yield the expected outcomes under varying load conditions. The PSO tuned controller provides better results as compared to traditional tuning methods. The switching scheme is implemented using hysteresis controller to control the SAPF. The main objectives of this approach are to extract the compensating currents and cancel out the harmonics produced by balanced, unbalanced and nonlinear loads. The planned scheme is designed and implemented in MATLAB/Simulink and then its performance on a developed laboratory prototype is validated experimentally.

INDEX TERMS Harmonic mitigation, hysteresis current controller, particle swarm optimization, PI controller, power quality shunt active power filter, synchronous reference frame theory.

NOMENCLATURE

ADALINE	Adaptive Linear Neuron.
ADC	Analog to Digital Converter.
ANN	Artificial Neural Network.
CDC	DC-link Capacitor.
C_f	Ripple Filter Capacitor.
d_n	Switching Function.
DAC	Digital to Analog Converter.
DSTATCOM	Distribution Static Compensator.
e	Error.
FLC	Fuzzy Logic Control.
FPGA	Field Programmable Gate Array.
g_n	Switching Function
i_c	Compensating Current.
i_n	Harmonic Current.
i_{La}, i_{Lb}, i_{Lc}	Load Currents.
IRPT	Instantaneous Reactive Power Theory.
i_s	Source Current.
i^*_{sa}, i^*_{sb}, i^*_{sc}	Reference Compensating Currents.
i_{sa}, i_{sb}, i_{sc}	Actual Source Current.
ISE	Integral Square Error.
i_d, i_q	Direct and Quadrature Axis Current.
k	Overloading Factor.
K_p	Proportional Gain.
K_i	Integral Gain.
L_c	Filter Inductor.
m_i	Modulation Index.
MPPT	Maximum Power Point Tracking.
n	n^{th} Harmonic Order.
PCC	Point of Common Coupling.
p_f (t)	Active Power.

The associate editor coordinating the review of this manuscript and approving it for publication was Nagesh Prabhu.

p_r (t)	Reactive Power.
p_h (t)	Harmonic Power.
PID	Proportional Integral Derivative.
PLL	Phase Lock Loop.
PSO	Particle Swarm Optimization.
PV	Photovoltaic.
R_f	Ripple Filter Resistance.
SAPF	Shunt Active Power Filter.
SRF	Synchronous Reference Frame.
THD	Total Harmonic Distortion.
UPQC	Unified Power Quality Conditioner.
V_{sa}, V_{sb}, V_{sc}	Source Voltages.
V_{pa}, V_{pb}, V_{pc}	Point of Common Coupling Voltages.
V_{1M}, V_{2M}, V_{3M}	Compensating Voltage.
V_{dc}	DC Link Voltage.
V_{dc}*	Reference DC Link Voltage.
VSI	Voltage Source Inverter.
ω	Angular Frequency.
Δ_iL	Ripple Filter Inductance.
Δt	Minimum Time Required for Attaining Steady State After a Disturbance.
%	Percentage.

I. INTRODUCTION

The distribution systems in this era of advanced power electronics are suffering from the issues related to power quality. The application of power electronics based nonlinear load is increasing which increases the harmonics in the distribution system. The industrial (paper mills, arc furnaces, automotive, metals, cement etc.) and non-commercial (refrigerators, washing machines, televisions etc.) appliances contribute fairly to the harmonics injection into the grid which results in reducing the power factor [1]–[4]. The inferior quality of the power is responsible for power loss, resonance, errors in readings of the instruments, etc. The consumer and the utility are paying heavily for these losses. The power quality issues are of serious concern and require a lot of focus and extensive work to improve [5]. The harmonic voltage compensation purposes have been shown in single-phase APF [6], [7] allowing loads to be supplied by a nearly sinusoidal voltage.

Many furnace industries till date are using the passive filters to suppress harmonics, but these filters have disadvantages such as resonance, large size, aging, compensation, and their inability to compensate for unbalanced loads [8]. To mitigate these problems, the shunt active power filter (SAPF) came out as an effective solution. The SAPF can compensate for current-related issues, while the series APF can compensate for voltage-related issues, and the unified power quality conditioner (UPQC) can reduce both voltage and current harmonics [9], [10]. Moreover, they have the capability for load balancing in case of three-phase active filters and reactive power compensation.

The dynamic performance of a SAPF is reliant on how rapidly and precisely the harmonic components are extracted from the load current. The harmonic extraction techniques namely instantaneous reactive power theory (IRPT) also known as the p-q theory [11], [12] and synchronous reference frame (SRF) theory also known as d-q theory are given in [13], [14]. The SRF theory performs excellently for eliminating the harmonics in real-time systems. The dynamic performance of SAPF depends upon the converter topology and DC link voltage regulation [15]. There are different approaches (controllers) to control the DC link voltage like proportional integral derivative (PID) [16], fuzzy logic control (FLC) [17], artificial neural network (ANN) approach and genetic algorithm method (GA) [18] etc. In addition, [19] discusses the different control techniques for SAPF. The adaptive DC-link voltage control for SAPFs was introduced by Juan *et al.* [20], which minimized switching loss during operation. They used predictive current control and proportional voltage control to maintain the DC-link voltage. Under unbalanced and distorted supply voltage conditions, Xiaohua *et al.* [21] presented a current reference control approach for SAPF that uses the Kalman filter to extract the harmonic content.

The PSO algorithm is a dominant tool for optimization of nonlinear functions. The method was found through simulation of a simplified social model inspired by the flocking of birds [22], [23] and presently being used in many applications for optimization of nonlinear equations. The selective harmonic elimination method is performed using PSO to calculate the switching angles to eliminate the harmonics [24]. The harmonics alleviation and DC link voltage regulation using PSO have been employed to find out the gains of PI controller in SAPF [25]. In SAPF control strategy, a low pass filter was used to eliminate the ripple content by using wavelet and adaptive filter based control strategy in [26]. PI controller is the most popular industrial controller and is used by 95% of process industries [27]. The major drawback of PI controller is the requirement of having a precise linear mathematical model of the system, which is difficult to obtain under varying parameters and non-linear load disturbances.

Photovoltaic (PV) integrated SAPF mitigates power quality issues in a distribution system while simultaneously lowering reliance on fossil fuels, resulting in enhanced environmental quality. The presented system uses a fuzzy logic proportional integrator derivative multiple complex coefficient filter multiple second-order generalized integrator frequency-locked loop. The maximum power from the PV panel is tracked using the PSO-based perturb and observe technique under changing external environment in the study [28]. PV integrated DSATCOM to resolve the power quality issues caused by nonlinear loads demonstrated in [29] to track the peak power point, an FLC-based maximum power point tracking (MPPT) controller was used.

Battery energy storage system and PV with UPQC can be a good distributed generating solution for improving the power quality of today's modern power system [30]. Mukundan *et al.* [31] demonstrates a grid-connected PV system that uses a binary hybrid multilevel inverter and a damped second-order generalized integral controller. The

universal APF system enhances voltage and current quality by combining both shunt and series APF introduced in [32]. To improve power quality, a PV-based SAPF system with a Perturb and Observe MPPT controller and a non-linear load is connected [33]. Fuzzy PSO strategy with a PV fed SAPF to improve power quality and provide clean electricity [34].

To generate pulse width modulation (PWM) signals for driving SAPF, the linear and non-linear control strategies for tracking the harmonic current were presented in [35]. The nonlinear current control technique mainly consists of hysteresis control and predictive control. One of the most appropriate PWM switching methods for producing reference current in SAPF is hysteresis current control. The advantages of hysteresis current control include high stability, speed, and accuracy in dynamic behavior. In linear current control, techniques such as sinusoidal PWM, deadbeat control and ramp comparison control, etc. are used to obtain the PWM signal [36].

The proposed PSO-PI control algorithm is compared with ref. [37] which only considers nonlinear load conditions whereas proposed approach deals with different combinations of balanced, unbalanced and nonlinear load condition. The proposed PSO-PI algorithm is worked out on 30μs sampling time against 52.5ms used in [38], [39] therefore the proposed scheme is fast and offers lesser computational burden and lesser THD.

In this paper, a three-phase SAPF to enhance power quality in the distribution system is proposed. The combination of linear and nonlinear load demands for reactive power and current harmonic compensation. The SRF method always proves to be superior to IRPT strategies for current compensation under non-ideal conditions of voltage.

In this work, time-domain based SRF theory is applied to control the system. A PSO tuned PI controller is incorporated with SRF theory. The hysteresis current control technique is applied for generating the gate pulses of the VSI (SAPF). This control strategy is experimentally implemented as a prototype in the laboratory. This work is executed with microsecond time step on FPGA based computational engine of OPAL-RT. The performance of the SAPF and current control strategies has been evaluated in terms of harmonic mitigation and DC link voltage regulation. The results with classically tuned and PSO tuned controller are presented here.

The key contributions of this article are as follows:

- Shunt active power filter is employed to improve the power quality.
- Mathematical modeling of the proposed system is formulated.
- Particle swarm optimization-based control strategy is utilized here which enhances the system performance as compared to classical techniques.
- OPAL-RT which has FPGA based computational engine with microsecond time step size, is applied here as a hardware controller.
- A prototype of the proposed shunt active power filter is developed and tested in the laboratory.
- The developed control algorithm is used to regulate the SAPF and it can improve various elements of power quality including harmonics mitigation and load balancing.
- Costs and benefits of the proposed and traditional control techniques have been compared.

This paper is organized as follows. In section 2, the configuration of SAPF is given. In section 3, SRF theory using the PSO/PI controller is described. Experimental results are shown in section 4. Finally, the conclusion is provided in section 5.

II. SYSTEM CONFIGURATION OF SAPF

The fundamental compensation principle of SAPF is shown in Fig. 1. When SAPF is not active, the source and load currents both carry the same harmonics (i.e., their signatures are same). Once the SAPF is connected at PCC, it injects controlled compensating current to make the supply current free of harmonics irrespective of the load characteristics. The utility voltage is given by eqn. (1)

$$v_s(t) = v_m sin\omega t \tag{1}$$

The instantaneous source currents at PCC are given by eqn. (2)

$$i_s(t) = i_L(t) - i_c(t) \tag{2}$$

The load current i_L with fundamental and harmonics components is represented in eqn. (3)

$$i_L(t) = \sum_{n=1}^{\infty} i_n sin(n\omega t + \phi_n) = i_1 sin(\omega t + \phi_1) + \sum_{n=2}^{\infty} i_n sin(n\omega t + \phi_n) \tag{3}$$

Instantaneous load power can be given as eqn. (4)

$$\begin{aligned} p_L(t) &= v_s(t) * i_L(t) = v_m i_1 sin^2\omega t * cos\phi_1 + v_m i_1 sin\omega t \\ &\quad * cos\omega t * sin\phi_1 \\ &\quad + v_m sin\omega t * \sum_{n=2}^{\infty} i_n sin(n\omega t + \phi_n) \qquad (4) \\ &= p_f(t) + p_r(t) + p_h(t) \qquad (5) \end{aligned}$$

where, $p_f(t)$ is the active power, $p_r(t)$ is the reactive power and $p_h(t)$ is the harmonic power.

Also,

$$p_f(t) = v_m i_1 sin^2\omega t * cos\phi_1 = v_s(t) * i_s(t) \tag{6}$$

From eqn. (6) the source current supplied after compensation, is expressed as in eqn. (7)

$$i_s(t) = \frac{p_f(t)}{v_s(t)} = i_1 cos\phi_1 sin\omega t = i_{sm} sin\omega t \tag{7}$$

where $i_{sm} = i_1 cos\phi_1$

The control law must consider an extra current to the capacitor leakage and converter switching losses. The following

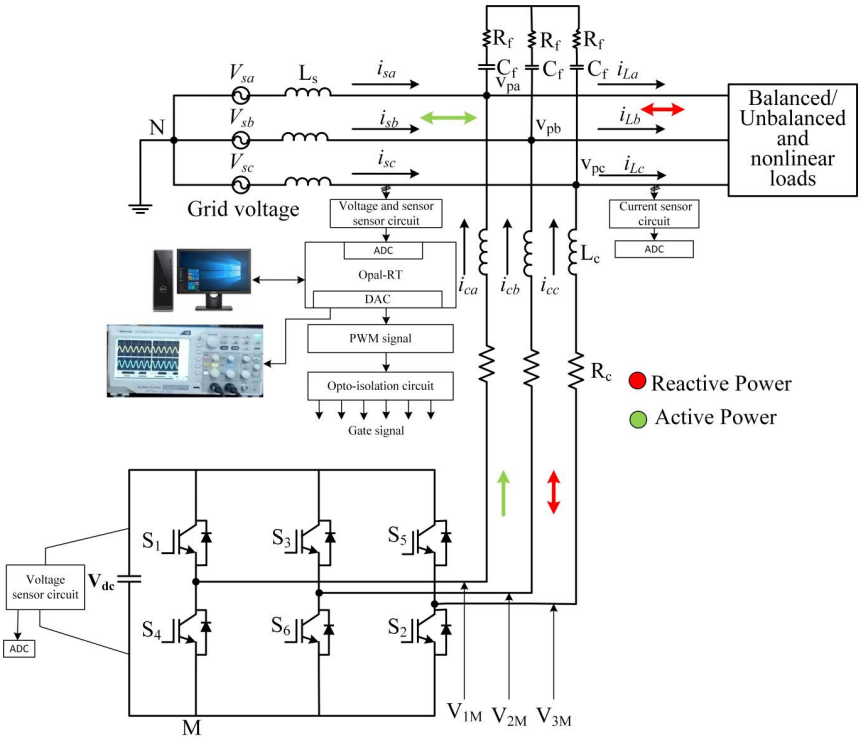

FIGURE 1. Power circuit of SAPF.

compensation current must be provided by the SAPF in eqn. (8):

$$i_c(t) = i_L(t) - i_s(t). \tag{8}$$

A. DESIGN OF PROPOSED SYSTEM CONFIGURATION

The proposed SAPF system is shown in Fig.1. To design a required SAPF, the values of few parameters need to be chosen and are as follows:

Three-phase grid voltage (V_s) 58V (L-L), frequency (f) 50Hz, load current (i_L) 5A. The nonlinear load is a combination of three-phase diode rectifier with RL load. The SAPF is designed based on the analysis available in [40], [41] and their parameters are derived as below:

In three-phase diode rectifier, the supply current (i_s) is a quasi-square waveform given in eqn. (9)

$$i_s = i_L\sqrt{\frac{2}{3}} \tag{9}$$

The value of the fundamental component of the quasi-square waveform is expressed as in eqn. (10)

$$i_{s1} = \frac{\sqrt{6}}{\pi} i_L \tag{10}$$

The current rating (harmonic current) of SAPF is given in eqn. (11)

$$i_{SAPF} = i_c = i_h = \sqrt{i_s^2 - i_{s1}^2} \tag{11}$$

The power rating of SAPF (S) is given in eqn. (12)

$$S = 3V_s i_c \tag{12}$$

The DC-link voltage of SAPF is given by eqn. (13)

$$V_{dc} = \frac{2\sqrt{2}\, V_s}{m_i} \tag{13}$$

where 'm_i' is the modulation index and 'V_s' is the phase voltage.

The compensating inductance of SAPF is given in eqn. (14)

$$L_c = \frac{\sqrt{3}\Big/2m_i V_{dc}}{6kf\,\Delta I_f} \tag{14}$$

where '$6k$' is the overloading factor, f is the switching frequency and ΔI_f is the ripple factor. The DC-link capacitor is calculated from change in stored energy and is given by eqn. (15)

$$\begin{aligned} \Delta E &= \frac{1}{2} C_{dc}\left(V_{dc}^2 2 - V_{dc}^2 2_{ref}\right) = 3V_s k i_c \Delta t, \\ C_{dc} &= \frac{3V_s k i_c \Delta_t}{0.5(V_{dc}^2 2 - V_{dc}^2 2ref)}. \end{aligned} \tag{15}$$

The proposed strategy is designed to minimize the THD and improve the power factor.

B. DYNAMIC SAPF MODEL

According to Fig.1, one can develop the dynamic model of three-phase SAPF. According to circuit theory and KVL,

we can obtain

$$V_{pa} = L_c \frac{di_{ca}}{dt} + R_c i_{ca} + V_{1M} + V_{MN} \quad (16)$$

$$V_{pb} = L_c \frac{di_{cb}}{dt} + R_c i_{cb} + V_{2M} + V_{MN} \quad (17)$$

$$V_{pc} = L_c \frac{di_{cc}}{dt} + R_c i_{cc} + V_{3M} + V_{MN} \quad (18)$$

where L_c and R_c are respectively SAPF inductance and resistance.

The V_{MN} is the voltage that is expressed as in eqn. between M and N in eqn. (19)

$$V_{MN} = -\frac{1}{3}\sum_{m=1}^{3} V_m M \quad (19)$$

A switching function g_n denotes the switch's ON / OFF state and is given in eqn. (20).

$$g_n = \begin{cases} 1, & if\ S_n\ is\ On\ and\ S_{n+3}\ is\ Off \\ 0, & if\ S_n\ is\ Off\ and\ S_{n+3}\ is\ On \end{cases} \quad (20)$$

where, n = 1,2,3.

As $V_{nM} = g_n V_{dc}$, the eqn. (16), (17), (18) becomes

$$\frac{di_{ca}}{dt} = -\frac{R_c}{L_c} i_{ca} + \frac{V_{pa}}{L_c} - \frac{V_{dc}}{L_c}\left(g_1 - \frac{1}{3}\sum_{m=1}^{3} g_m\right) \quad (21)$$

$$\frac{di_{cb}}{dt} = -\frac{R_c}{L_c} i_{cb} + \frac{V_{pb}}{L_c} - \frac{V_{dc}}{L_c}\left(g_1 - \frac{1}{3}\sum_{m=1}^{3} g_m\right) \quad (22)$$

$$\frac{di_{cc}}{dt} = -\frac{R_c}{L_c} i_{cc} + \frac{V_{pc}}{L_c} - \frac{V_{dc}}{L_c}\left(g_1 - \frac{1}{3}\sum_{m=1}^{3} g_m\right) \quad (23)$$

Now, d_n can be defined as:

$$d_n = g_n - \frac{1}{3}\sum_{m=1}^{3} g_m \quad (24)$$

It is obvious that d_n varies with the g_n switching function, i.e., nonlinearity of the proposed system. Based on eqn. (24) and one may acquire eight permissible IGBT switching states

$$\begin{bmatrix} d_1 \\ d_2 \\ d_3 \end{bmatrix} = \frac{1}{3}\begin{bmatrix} 2 & -1 & -1 \\ -1 & 2 & -1 \\ -1 & -1 & 2 \end{bmatrix}\begin{bmatrix} g_1 \\ g_2 \\ g_3 \end{bmatrix} \quad (25)$$

Then eqn. (21), (22), (23) becomes

$$\frac{di_{ca}}{dt} = -\frac{R_c}{L_c} i_{ca} + \frac{V_{pa}}{L_c} - \frac{V_{dc}}{L_c} d_1 \quad (26)$$

$$\frac{di_{cb}}{dt} = -\frac{R_c}{L_c} i_{cb} + \frac{V_{pb}}{L_c} - \frac{V_{dc}}{L_c} d_2 \quad (27)$$

$$\frac{di_{cc}}{dt} = -\frac{R_c}{L_c} i_{cc} + \frac{V_{pc}}{L_c} - \frac{V_{dc}}{L_c} d_3 \quad (28)$$

$$\text{Define} \begin{cases} x_1 = i_n \\ x_2 = i_{n1} \end{cases} \quad (29)$$

where $i_n = [i_{ca}; i_{cb}; i_{cc}]$

Putting eqn. (29) into (26), (27), (28), we have

$$x_1 = n_1 = -\frac{R_c}{L_c} i_n + \frac{V_n}{L_c} - \frac{V_{dc}}{L_c} d_n \quad (30)$$

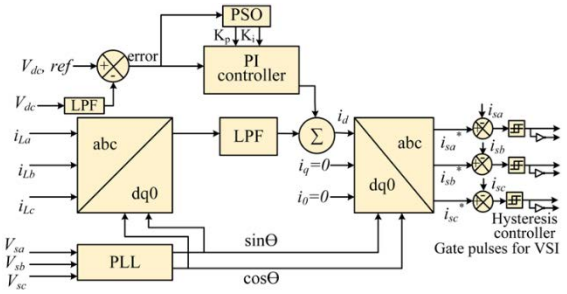

FIGURE 2. Block diagram of SRF based control technique.

$$x_2 = i_{n1} = -\frac{R_c}{L_c} i_n + \frac{dV_n}{dt}\frac{1}{L_c} - \frac{1}{L_c}\frac{dV_{dc}}{dt} d_n \quad (31)$$

$$= -\frac{R_c^2}{L_c^2} i_n - \frac{R_c}{L_c^2} v_n + \frac{1}{L_c}\frac{dV_n}{dt} + \left(\frac{R_c}{L_c^2} V_{dc} - \frac{1}{L_c}\frac{dV_{dc}}{dt}\right) dn. \quad (32)$$

Then eqn. (32) becomes

$$x_2 = b_a(x) + M_z$$

where $b_a(x)$ and M_z represented the state control.

$$b_a(x) = \frac{R_c^2}{L_c^2} i_n - \frac{R_c}{L_c^2} v_n + \frac{1}{L_c}\frac{dV_n}{dt}, M = \frac{R_c}{L_c^2} V_{dc} - \frac{1}{L_c}\frac{dV_{dc}}{dt} \quad (33)$$

$$z = d_n, v_n = \left[V_{pa}; V_{pb}; V_{pc}\right], d_n = [d_1; d_2; d_3]. \quad (34)$$

III. SYNCHRONOUS REFERENCE FRAME THEORY PSO BASED PI CONTROLLER

The synchronous reference frame (SRF) theory is applied to control the harmonic compensation system in real-time. The functional diagram of SRF based control method is shown in Fig. 2.

The load currents (i_{La}, i_{Lb}, i_{Lc}) are detected as feedback signals and are transferred into d-q axis by Park transformation as given below in eqn. (35):

$$\begin{bmatrix} i_d \\ i_q \\ i_0 \end{bmatrix} = \frac{2}{3}\begin{bmatrix} cos\theta & -sin\theta & \frac{1}{2} \\ cos\left(\theta - \frac{2\pi}{3}\right) & -sin\left(\theta - \frac{2\pi}{3}\right) & \frac{1}{2} \\ cos\left(\theta + \frac{2\pi}{3}\right) & -sin\left(\theta + \frac{2\pi}{3}\right) & \frac{1}{2} \end{bmatrix}\begin{bmatrix} i_{La} \\ i_{Lb} \\ i_{Lc} \end{bmatrix} \quad (35)$$

These signals are synchronized with point of common coupling (PCC) using phase locked loop (PLL). The PLL is required to extract the phase information of a periodic and physical control.

Generally, the physical control has unpredictable variations and it has to dynamically ensure the accuracy of phase information extracted. Pure sine and cosine waves need to be generated that are synchronized to the grid voltage to perform the abc to $d-q$ and the $d-q$ to abc transformations. The components are cleared through a LPF to remove the DC

segments of i_d and i_q in eqn. (36), (36). The d-axis and q-axis currents consist of fundamental and harmonic segments as follows:

$$\begin{aligned} i_d &= i_{d-DC} + i_{d-AC} \\ &= \frac{\sqrt{2}}{3}\left[i_{La}cos\left(\omega t\right) + i_{Lb}cos\left(\omega t - \frac{2\pi}{3}\right)\right. \\ &\quad \left. + i_{Lc}cos\left(\omega t + \frac{2\pi}{3}\right)\right] \end{aligned} \tag{36}$$

$$\begin{aligned} i_q &= i_{q-DC} + i_{q-AC} \\ &= \frac{\sqrt{2}}{3}\left[-i_{La}sin\left(\omega t\right) - i_{Lb}sin\left(\omega t - \frac{2\pi}{3}\right)\right. \\ &\quad \left. - i_{Lc}sin\left(\omega t + \frac{2\pi}{3}\right)\right] \end{aligned} \tag{37}$$

The $d-q$ to abc transformation is carried out to get three phase reference compensating currents $i^*_{sa}, i^*_{sb}, i^*_{sc}$. The expressions of these currents are given in eqn. (38), (39), (40):

$$i^*_{sa} = \frac{\sqrt{2}}{3}\left[i_{d,AC}cos\left(\omega t\right) - i_q sin\left(\omega t\right)\right], \tag{38}$$

$$i^*_{sb} = \frac{\sqrt{2}}{3}\left[i_{d,AC}cos\left(\omega t - \frac{2\pi}{3}\right) - i_q sin\left(\omega t - \frac{2\pi}{3}\right)\right], \tag{39}$$

and

$$i^*_{sc} = \frac{\sqrt{2}}{3}\left[i_{d,AC}cos\left(\omega t + \frac{2\pi}{3}\right) - i_q sin\left(\omega t + \frac{2\pi}{3}\right)\right] \tag{40}$$

A. PARTICLE SWARM OPTIMIZATION

As compared to classical tuning techniques, particle swarm optimization method can handle a multiple governing equations with constraints and yields an optimal solution for the targeted problem. PSO is an evolutionary computation method, which is inspired from social behavior movement and intelligent thought process of swarms through which they reach to an optimal location. Initialization of PSO is done by population of random solutions and random velocity is assigned to each solution. Random position values are used to initialize each particle. A repetitive process is employed to obtain the optimal values of PI controller parameters [42]–[43].

PSO involves identification of two premier feature movements of particles; 1) global particle-to-particle best outcome and 2) local particle's iteration-to-iteration for best solution. Iteration-to-iteration data denotes the 'pbest' the best solution it has reached upto this point. Particle-to-particle data brings about putting away the best outcomes reached by any particle, and is called 'gbest'. The 'pbest' and 'gbest' factors are called intellectual and social segments individually. After each iteration, 'pbest' and 'gbest' are refreshed for every particle, for reaching better solution and more dominating solution is found. 'pbest' and 'gbest' are iterated constantly till the point either the wanted outcomes are obtained or no promising solutions can be obtained in the given search space. Particle's velocity determines the direction and amount of movement.

TABLE 1. Parameters values of PSO alogirthm.

Parameter	Value
Maximum no. of iterations	50
Population size	15
Inertia	0.3
Damping ratio	0.95
Sampling time	30 e-6

The PSO defines every particle in D-dimensional space as $X_i = (x_{i1}, x_{i2}, \ldots, x_{iD})$, where the subscript '$i$' represents the number of particle and the second subscript represents the dimension, the number of parameters defining the solution. The previous best position is represented as $P_i = (p_{i1}, p_{i2}, \ldots, p_{iD})$ which is stored in the memory and the velocity for each dimension is independently established as $V_i = (v_{i1}, v_{i2}, \ldots, v_{iD})$.

After each iteration, the velocity term is updated, and the particle is moved with some randomness in the direction of its own best position, pbest, and the global best position, gbest. Velocity is updated as given by eqn. (41)

$$\begin{aligned} V_{id}^{(t+1)} = \omega \times V_{id}^{(t)} + U[0,1] \times \psi_1 \times (p_{id}^{(t)} - x_{id}^{(t)}) + U[0,1] \\ \times \psi_2 \times (P_{gd}^{(t)} - x_{id}^{(t)}) \end{aligned} \tag{41}$$

The position is updated using this velocity $V_{id}^{(t+1)}$ and given as eqn. (42).

$$X_{id}^{(t+1)} = X_{id}^{(t)} + V_{id}^{(t+1)} \tag{42}$$

where U [0,1] samples a uniform random distribution, t is a relative time index, ψ_1 and ψ_2 are weighted trade off and impacts of the local best and global best solutions' on the particle's total velocity.Table 1 shows the PSO parameters.

The undesirable losses such as overshoot, settling time, transient response and steady state error are minimized by using PI controller by maintaining a DC-link voltage. It is difficult to model a power system network using conventional mathematical approaches since it is complex, non-linear and non-stationary along with many inequality constraints. Therefore, by using various optimization techniques to optimize the PI controller coefficients; there can be further improvement in the compensation capability of SAPF. The proposed PSO algorithm flow chart of the PI controller is shown in Fig. 3.

In this paper, the PSO scheme has been used for the optimization of PI controller parameters K_p and K_i. The integral square error (ISE) performance index presented in eqn. (43) is used to optimize the objective function 'j' as follows:

$$j = \int_0^t e^2 dt \tag{43}$$

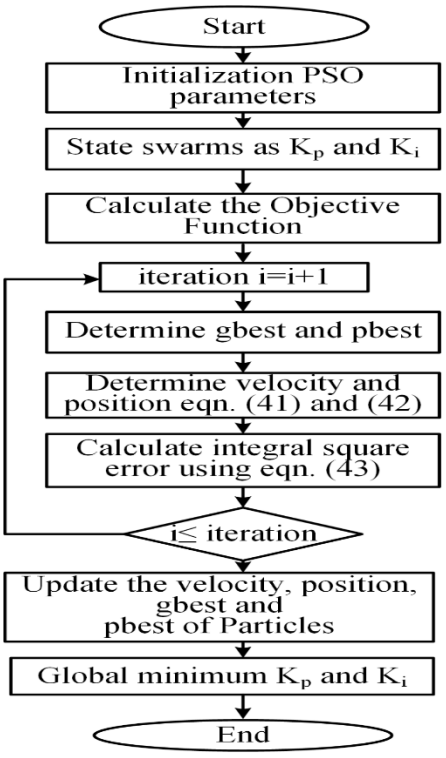

FIGURE 3. Flow chart of the PSO optimization technique for determining the optimal PI controller parameter value.

The coefficient K_p and K_i optimized at a different load condition such as balanced/unbalanced and nonlinear load conditions provide satisfactory performance for all conditions in the experimental system. The voltage of the DC-link capacitor is detected and compared to a reference voltage. As shown in Fig. 2, the error '$e = V_{dc}, ref - V_{dc}$' is minimized using PI controller, which provides output as an active current that corresponds to power flow needed to maintain DC-link voltage.

B. HYSTERESIS CURRENT CONTROL

The hysteresis current control method has been adopted to fire the IGBT of the SAPF. The significance of this control method is because of its fast current controllability, simple usage and stability in all conditions. The hysteresis comparator compares the current injected by the inverter with the reference current in order to provide switching gate pulses. These gate pulses are responsible to decide the turning on and off of the IGBTs.

IV. SIMULATION RESULTS AND DISCUSSION

Sim Power System toolbox in MATLAB/Simulink is used to simulate the proposed system under various load conditions. Table 2 lists all of the simulation parameters that were considered.

TABLE 2. Lists the parameters of the simulation.

Parameter	Value
Grid supply voltage (V_s)	58V (L-L)
Supply frequency (f)	50 Hz
DC-link capacitor (C_{dc})	2350 μF
Filter inductor (L_c)	4 mH
DC-link of PI gains	K_p=0.3, K_i=0.7
Ripple filter	R_f= 10 Ω, C_f=50 μF
Load	three-rheostat 100 Ω each, unbalanced load resistance is 100 Ω, 50 Ω, 10 Ω, three-phase uncontrolled diode rectifier with R = 15Ω and L = 50 mH

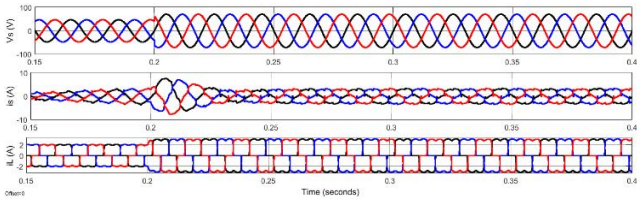

FIGURE 4. Sudden disturbance in the grid voltage (V_s).

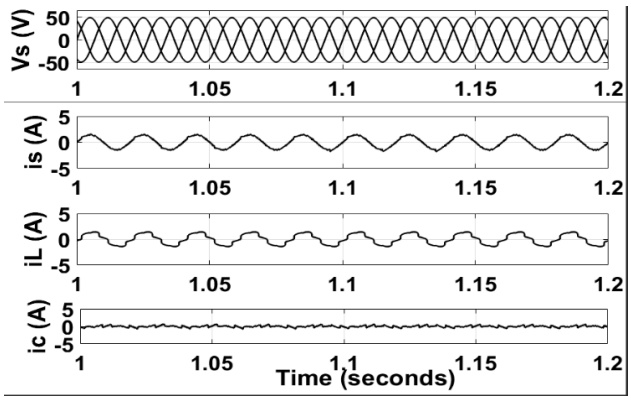

FIGURE 5. System performance under conditions of balanced and nonlinear load.

A. PERFORMANCE OF SYSTEM UNDER SUDDEN DISTURBANCE IN THE GRID VOLTAGE

The rapid disturbance in grid voltage is depicted in the Fig. 4. The grid voltages are perturbed for 0.2 seconds which results in grid current disturbances. Despite the fact that source currents had overshot by 40% it gets settle down in just three cycles which shows the effectiveness of the proposed method.

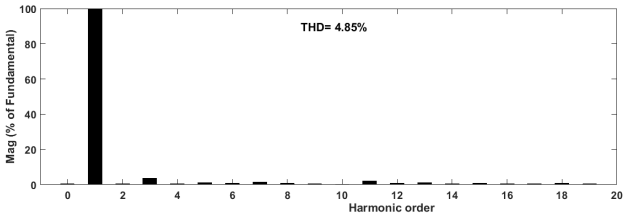

FIGURE 6. Harmonic spectrum of source current.

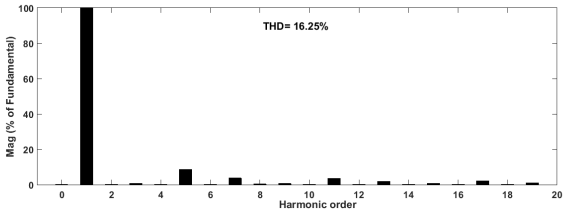

FIGURE 7. Harmonic spectrum of load current.

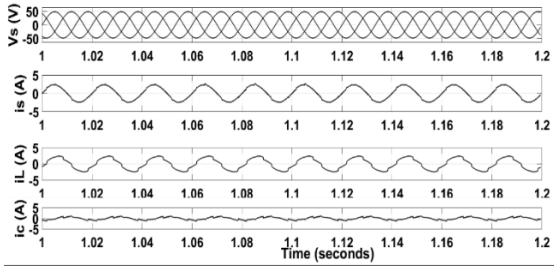

FIGURE 8. System performance under conditions of unbalanced and nonlinear load.

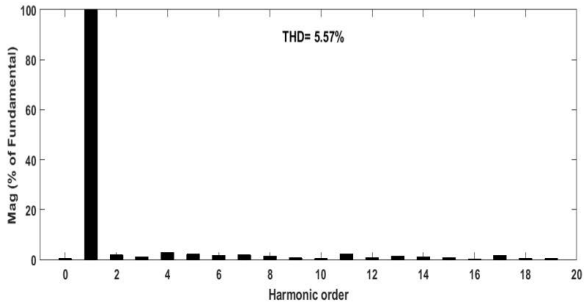

FIGURE 9. Harmonic spectrum of source current.

B. PERFORMANCE OF SYSTEM UNDER BALANCED AND NONLINEAR LOAD CONDITIONS

Fig.5 shows the grid voltage, grid current, load current and compensating current respectively when balanced and nonlinear load is applied. Figs. 6 and 7 provide the harmonic spectrum of source current and load current respectively. The THD has been reduced from 16.25% to 4.85%.

C. PERFORMANCE OF SYSTEM UNDER UNBALANCED AND NONLINEAR LOAD CONDITIONS

Fig.8 shows the source voltage, source current, load current and compensating current respectively when unbalanced and nonlinear load is applied. The harmonic spectrum of source current and load current is shown in Figs. 9 and 10, respectively. The THD has been decreased from 18.76% to 5.57%.

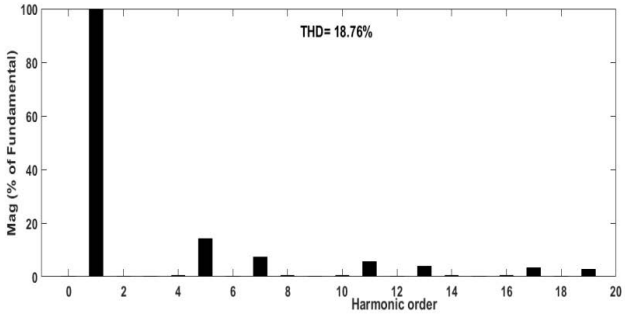

FIGURE 10. Harmonic spectrum of load current.

V. EXPERIMENTAL RESULTS AND ANALYSIS

The experimental setup of the proposed system is shown in Fig.11. Here, the PSO tuned PI controller is employed to control the SAPF for harmonic reduction. The lab prototype SAPF consists of Semikron IGBT module and three interfacing inductors of the desired value. The algorithms are implemented through the OPAL-RT 4510 system. The OPAL-RT 4510 has kintex-7 FPGA based high performance processor and advanced features such as higher number of I/O pins and in built analog to digital converter (ADC). The grid voltage signals are sensed by a potential transformer, the source & load currents are sensed by a current transformer and DC capacitor voltage is sensed by LV20P-LEM Hall Effect sensors. These sensed signals are applied to the ADC of the OPAL-RT through a signal-conditioning card. The entire control strategy is firstly simulated in MATLAB and then a Simulink model is created using RT library to comply with the RT lab. The RT lab is used to implement the proposed control algorithm on the host computer in the real-time system. This control algorithm finally controls the entire system on the actual hardware as shown in Fig.11. Table 3 lists all of the simulation parameters that were considered. The performance of SAPF for various cases is given below.

A. PERFORMANCE OF SAPF UNDER BALANCED & NONLINEAR LOAD WITHOUT PSO

Fig.12 shows the results without compensation i.e., when SAPF is not activated. It is expected that the actual source current and load current are the same without compensation, and that the THD is the same 23.90%. The DC-link voltage (V_{dc}) is 75V, source voltage (V_s) is 33V and actual source current (i_s) is 2.18A. The reference source current (i_s^*) is approximately same as actual source current. It is observed that the source current is distorted without compensation.

Fig.13 shows the waveforms when SAPF is activated and controlled using the classically tuned PI controller. The DC-link voltage is regulated to 95.4V. The source current is now almost harmonics-free & thus validates the capabil-

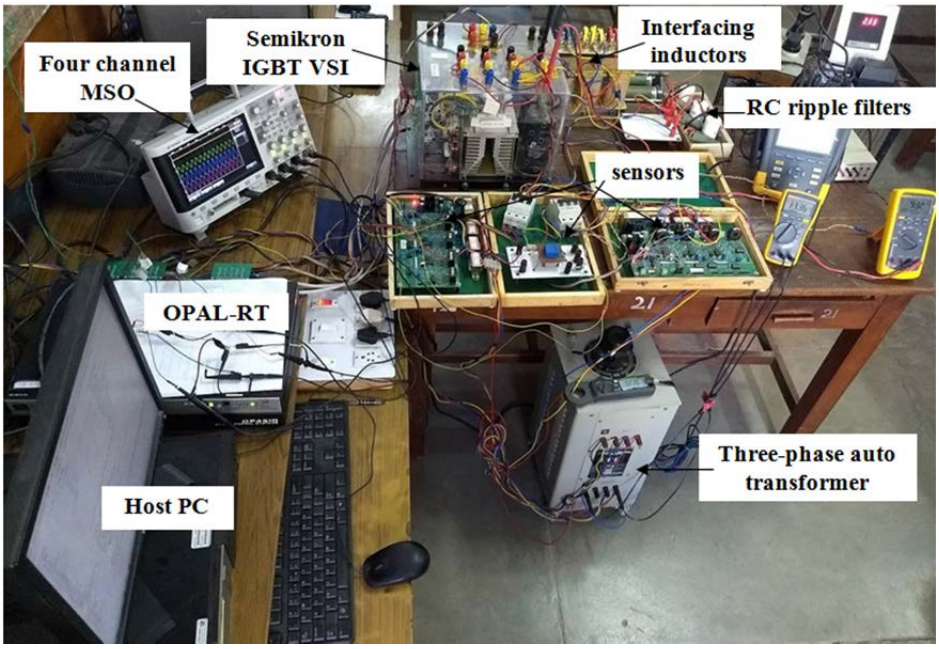

FIGURE 11. Lab prototype of experimental system.

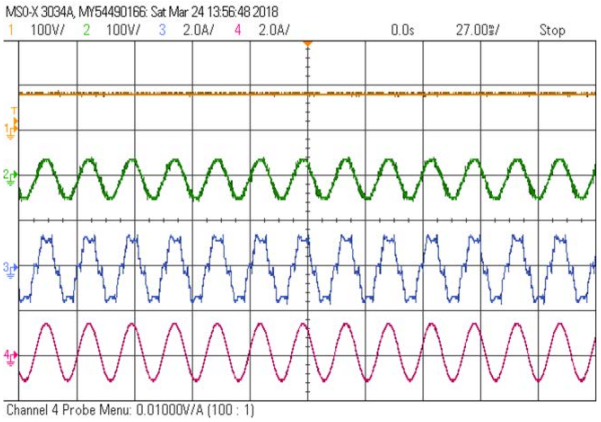

FIGURE 12. Experimental results without the compensation. Scale-CH1 V_{dc}:100 V/div, CH2 V_s: 100 V/div, CH3 i_s: 2A/div, CH4 i_s^*: 2A/div.

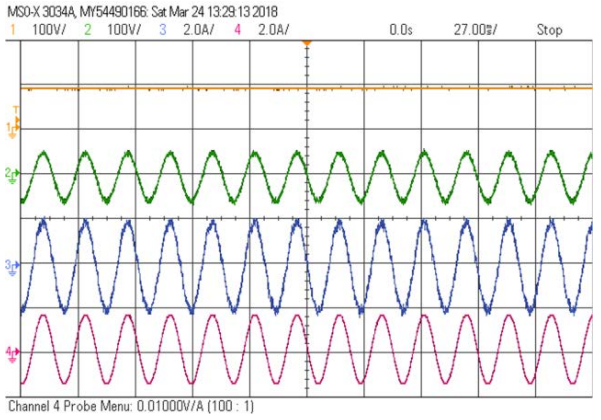

FIGURE 13. Experimental results with the compensation. Scale-CH1 V_{dc}:100 V/div, CH2 V_s: 100 V/div, CH3 i_s: 2A/div, CH4 i_s^*: 2A/div.

ity of the proposed SAPF to mitigate harmonics. Quantitatively, the simulation and experimental results are almost identical.

B. PERFORMANCE OF SAPF UNDER UNBALANCED & NONLINEAR LOAD WITHOUT PSO

The performance of SAPF is evaluated under unbalanced & nonlinear load conditions (the values of loads are given in appendix) and the results obtained are shown in Fig.13. The results obtained are using classically tuned PI controller. As per Fig.14, the value of DC-link voltage (V_{dc}) is 83.4V, source voltage (V_s) is 33V, source current (i_s) value is 2.40A and reference source current (i_s^*) is approximately same as actual source current.

C. PERFORMANCE OF SAPF UNDER BALANCED & NONLINEAR LOAD USING PSO-PI TECHNIQUE

In this approach, the controller is tuned with PSO. Fig.15 the response of SAPF when nonlinear and balanced load is applied. The value of DC-link voltage (V_{dc}) is 99.2V, source voltage (V_s) is 33V, source current (i_s) is 2.20A and the value of reference source current (i_s^*) is approximately same as actual source current.

Fig.16 and Fig.17 show the harmonic spectrum of load and source currents under balanced & nonlinear load without PSO. The THD is reduced to 4.88 %. Fig.18 represents the harmonic spectrum of source current using unbalanced load condition without PSO. The THD in this case is 5.72%, which is more than the balanced load case.

TABLE 3. Lists the parameters of the experimental validation.

Parameter	Value
Grid supply voltage (V_s)	58V (L-L)
Supply frequency (f)	50Hz
DC-link capacitor (C_{dc})	2350 μF
Filter inductor (L_c)	4 mH
DC-link of PI gains	K_p=0.015, K_i=0.001
Ripple filter	R_f= 10 Ω, C_f=50 μF
DC bus voltage, the LPF cutoff frequency	12 Hz
PCC voltage magnitude, the cutoff frequency of the LPF	10Hz
Sensor	LV20P-LEM
Load	three-rheostat 100 Ω each, unbalanced load resistance is 100 Ω, 50 Ω, 10 Ω, three-phase uncontrolled diode rectifier with R = 15Ω and L = 50 mH

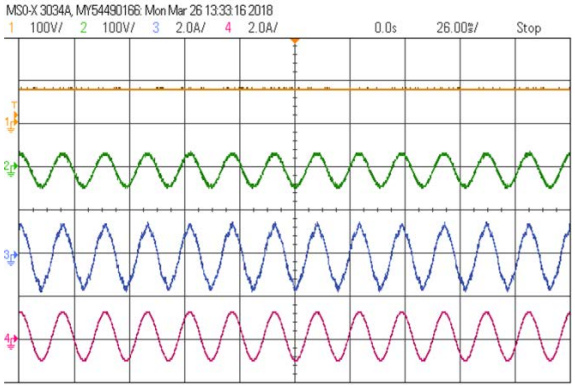

FIGURE 14. Experimental results with unbalanced load & nonlinear load. Scale-CH1 V_{dc}:100 V/div, CH2 V_s: 100 V/div, CH3 i_s: 2A/div, CH4 i_s*: 2A/div.

D. PERFORMANCE OF SAPF UNDER UNBALANCED & NONLINEAR LOAD USING PSO-PI TECHNIQUE

Fig.19 highlights the performance of SAPF when unbalanced and nonlinear load is applied and controller is tuned using PSO. The obtained DC-link voltage (V_{dc}) is 96V, source voltage (V_s) is 33V, source current (i_s) is 2.30A and reference source current (i_s^*) is approximately same as the actual source current. Fig.20 represents the harmonic spectrum of source current under balanced load using PSO-PI technique.

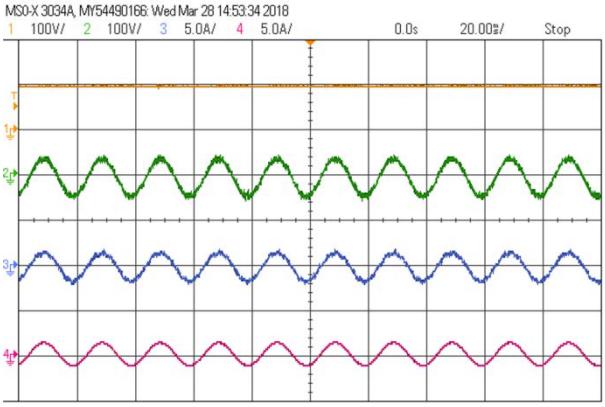

FIGURE 15. Experimental results balanced & nonlinear load. Scale-CH1 V_{dc}:100 V/div, CH2 V_s: 100 V/div, CH3 i_s: 5A/div, CH4 i_s*: 5A/div.

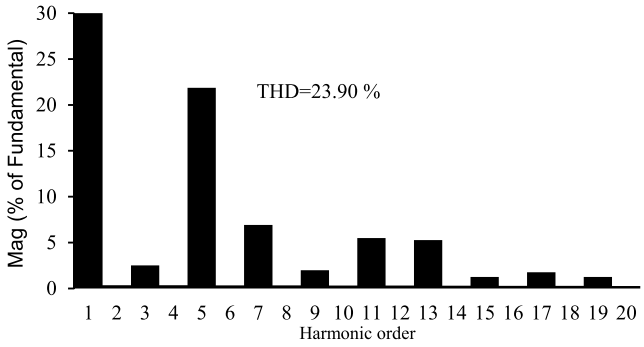

FIGURE 16. Harmonic spectrum of load current.

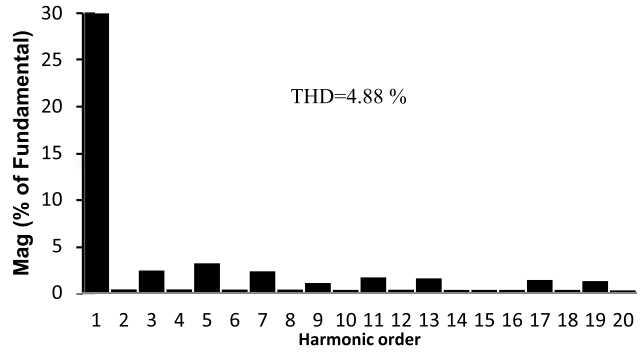

FIGURE 17. Harmonic spectrum of source current under balanced & nonlinear load without PSO.

Fig. 21 shows the harmonic spectrum of source current under unbalanced load using PSO-PI technique.

Fig. 22 represents the THD profile; (i) using MATLAB Simulation for balanced and non-linear lad conditions, (ii) Using MATLAB Simulation for unbalanced and non-linear load conditions, (iii) for experimental validation using conventional PI control for balanced and non-linear load conditions, (iv) for experimental validation using conventional PI control for unbalanced and non-linear load conditions, (v) for experimental validation using PSO-PI control for balanced and non-linear load conditions and (vi) for

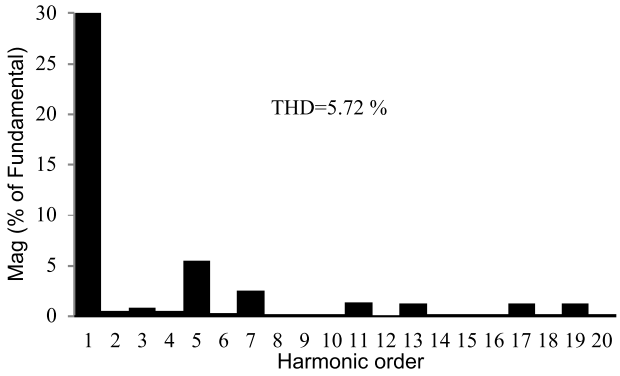

FIGURE 18. Harmonic spectrum of source current using under unbalanced & nonlinear load without PSO.

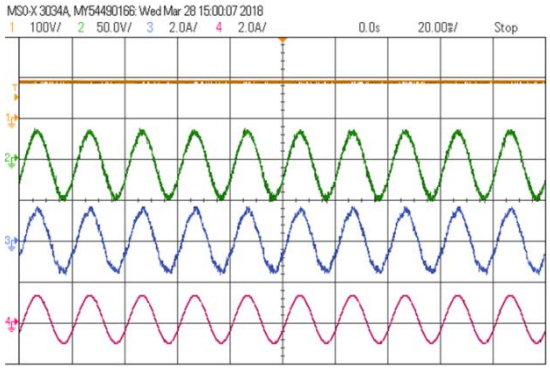

FIGURE 19. Experimental results unbalanced & nonlinear load. Scale-CH1 V_{dc}:100 V/div, CH2 V_s: 100 V/div, CH3 i_s: 2A/div, CH4 i_s*: 2A/div.

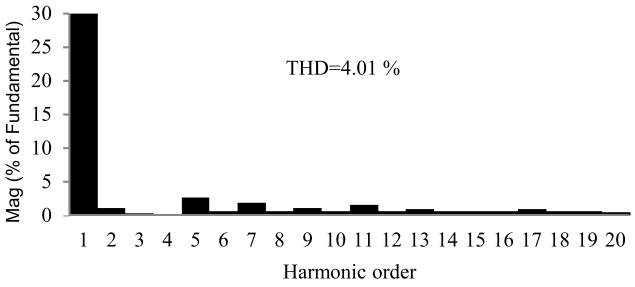

FIGURE 20. Harmonic spectrum of source current under balanced load using PSO-PI technique.

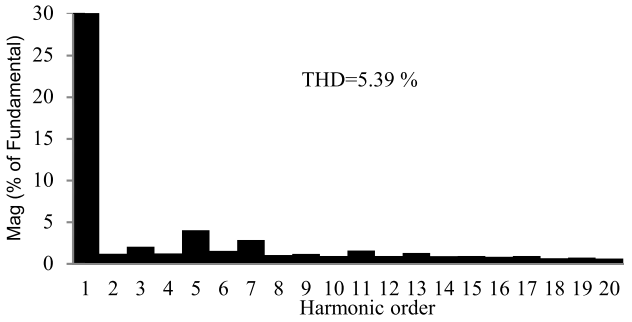

FIGURE 21. Harmonic spectrum of source current under unbalanced load using PSO-PI technique.

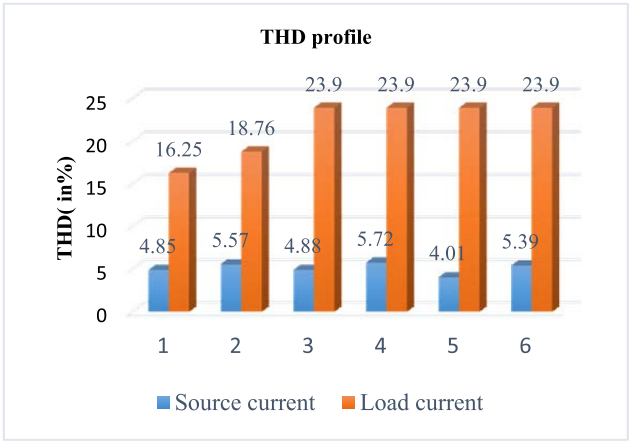

FIGURE 22. SAPF source current and load current THD profiles.

experimental validation using PSO-PI control for unbalanced and non-linear load conditions.

It is inferred that the THD profile of the experimental study has a similar feature to that of the simulation results. From the experimental results, it is seen that PSO-PI controller beats the performance of PI controller and offers lesser error, reduced overshoot (constant DC-link voltage) and lesser THD. Tables 4 and 5 show the indices for measuring SAPF efficiency, such as settling time (t_s), maximum overshoot (V_{dc} max), and source current THD values for balanced/unbalanced and nonlinear load condition.

E. COST BENEFIT ANALYSIS OF HARMONIC REDUCTION

The harmonics are responsible for power losses and their compensation leads to improved power quality and recovering in revenue saving. SAPF eliminates the harmonics but the deciding factor is their feasibility and cost. Various producers are looking for cost-effective ways to decrease harmonics inside electronic equipment. This section details the financial feasibility of SAPFs which is inspired from Key TS *et al.* [30]. To calculate the energy-loss incurred because of harmonics, a wiring model was developed [44]. The PCC can be selected in a building/industrial plant/ electrical distribution system to minimize the harmonics [45], [46]. Depending on the levels of harmonics, energy savings vary from 1 to 15%.

The comparison in terms of losses and savings for both compensated systems and non-compensated systems with different control techniques has been provided in Table 5. The analysis carried out for an SAPF of 0.405 kVA rating (lab proptotype) with a load of 1.155kW. The commercial cost of energy (in India) is considered at Rs. 8/kWh and the loading period is assumed to be 12 Hrs. The THD for compensated system (simulation) with balanced and nonlinear load condition using; PI is 5.20%, and PSO-PI is 4.85% whereas with unbalanced and nonlinear load condition using PI is 5.8%, and PSO-PI is 5.57%. The THD for compensated system (experimental) with balanced and nonlinear load

TABLE 4. Comparison of SAPF response under unbalanced supply condition using experimental testing.

Case	Maximum overshoot (ΔV_{dcmax}) in volts	V_{dc} transient settling time (t_s) in second	Source current THD in %
Without SAPF	-	-	23.9
SAPF with conventional PI	118 V	0.050	5.72
SAPF with PSO-PI	99 V	0.025	5.39

TABLE 5. Comparison of savings in revenue-loss.

Control Technique	Balanced and nonlinear load			Unbalanced and nonlinear load		
	Total losses without compensation (W)	Total losses with compensation (W)	Saving per year ($)	Total losses without compensation (W)	Total losses with compensation (W)	Saving per year ($)
PI (Simulation)	130	60	32.48	217	67	69.64
PSO-PI (Simulation)	130	56	34.34	217	64	71.03
PI (Experimental)	276	57	101.66	278	66	98.41
PSO-PI (Experimental)	276	47	106.31	278	62	100.27

condition using PSO-PI controller is 4.01% whereas with unbalanced and nonlinear load condition, THD is 5.39%. The comparison of savings in revenue loss is depicted in Table 5. It has been concluded that PSO-PI based control strategy delivers minimum losses and maximum savings. These savings are at very low power applications and will be amounting to a huge sum if applies to high power/industry applications.

Thus, SAPF; enhances power quality, minimizes harmonics induced energy losses, stabilizes voltage conditions, eradicates power factor penalties, advances system performance and productivity. In the above analysis, outstanding financial benefits may arise due to increased business productivity and improved product quality.

Based on this analysis, it can be inferred that the cost of SAPF can be recovered within two years. The results obtained from the proposed design are encouraging and may be of interest to industries as well as commercial applications such as aviation, textile, pharmaceutical, telecommunications and metal, etc.

VI. CONCLUSION

In this work, hardware implementation of SRF theory based SAPF is demonstrated. The proposed system is tuned using PSO technique to get high degree of performance. The proposed SAPF performs satisfactorily in harmonic elimination, load balancing, and voltage regulation without any frequency deviation at PCC under balanced/unbalanced nonlinear loads. The control approach mitigates the harmonics and maintains SAPF DC-link voltage. The proposed laboratory prototype is controlled using OPAL-RT FPGA based computational engine that has much less execution time. The THD of source current is 23.90% in case of without compensation, which is reduced to 4.01% and 5.39% respectively in case of balanced & unbalanced and nonlinear loads using proposed control strategy on hardware. Thus, based on the experimental investigation, this paper confirms the feasibility of PSO tuned control strategies for practical applications in power quality improvements.

REFERENCES

[1] A. A. Alkahtani, S. T. Y. Alfalahi, A. A. Athamneh, A. Q. Al-Shetwi, M. B. Mansor, M. A. Hannan, and V. G. Agelidis, "Power quality in microgrids including supraharmonics: Issues, standards, and mitigations," *IEEE Access*, vol. 8, pp. 127104–127122, 2020, doi: 10.1109/ACCESS.2020.3008042.

[2] T. Tarasiuk, S. G. Jayasinghe, M. Gorniak, A. Pilat, V. Shagar, W. Liu, and J. M. Guerrero, "Review of power quality issues in maritime microgrids," *IEEE Access*, vol. 9, pp. 81798–81817, 2021, doi: 10.1109/ACCESS.2021.3086000.

[3] L. P. R. Nadimuthu, K. Victor, C. H. Basha, T. Mariprasath, C. Dhanamjayulu, S. Padmanaban, and B. Khan, "Energy conservation approach for continuous power quality improvement: A case study," *IEEE Access*, vol. 9, pp. 146959–146969, 2021, doi: 10.1109/ACCESS.2021.3123153.

[4] N. Abas, S. Dilshad, A. Khalid, M. S. Saleem, and N. Khan, "Power quality improvement using dynamic voltage restorer," *IEEE Access*, vol. 8, pp. 164325–164339, 2020, doi: 10.1109/ACCESS.2020.3022477.

[5] P. S. Sanjan, N. Gowtham, M. S. Bhaskar, U. Subramaniam, D. J. Almakhles, S. Padmanaban, and N. G. Yamini, "Enhancement of power quality in domestic loads using harmonic filters," *IEEE Access*, vol. 8, pp. 197730–197744, 2020, doi: 10.1109/ACCESS.2020.3034734.

[6] L. F. J. Meloni, F. L. Tofoli, A. J. J. Rezek, and E. R. Ribeiro, "Modeling and experimental validation of a single-phase series active power filter for harmonic voltage reduction," *IEEE Access*, vol. 7, pp. 151971–151984, 2019, doi: 10.1109/ACCESS.2019.2947917.

[7] R. Wang, B. Hu, S. Sun, F. Man, Z. Yu, and Q. Chen, "Linear active disturbance rejection control for DC side voltage of single-phase active power filters," *IEEE Access*, vol. 7, pp. 73095–73105, 2019, doi: 10.1109/ACCESS.2019.2920626.

[8] J. C. Das, "Passive filters—Potentialities and limitations," *IEEE Trans. Ind. Appl.*, vol. 40, no. 1, pp. 232–241, Jan. 2004, doi: 10.1109/TIA.2003.821666.

[9] S. Bhattacharya, T. M. Frank, D. M. Divan, and B. Banerjee, "Active filter system implementation," *IEEE Ind. Appl. Mag.*, vol. 4, no. 5, pp. 47–63, Sep. 1998.

[10] S. Bhattacharya and D. Divan, "Design and implementation of a hybrid series active filter system," in *Proc. 26th Annu. IEEE Power Electron. Spec. Conf.*, vol. 1, Jun. 1995, pp. 189–195.

[11] M. T. Benchouia, I. Ghadbane, A. Golea, K. Srairi, and M. E. H. Benbouzid, "Implementation of adaptive fuzzy logic and PI controllers to regulate the DC bus voltage of shunt active power filter," *Appl. Soft Comput.*, vol. 28, pp. 125–131, Mar. 2015, doi: 10.1016/j.asoc.2014.10.043.

[12] J. Mindykowski, X. Xu, and T. Tarasiuk, "A new concept of harmonic current detection for shunt active power filters control," *Measurement*, vol. 46, no. 10, pp. 4334–4341, 2013, doi: 10.1016/j.measurement.2013.06.009.

[13] S. Mikkili and A. K. Panda, "Real-time implementation of PI and fuzzy logic controllers based shunt active filter control strategies for power quality improvement," *Int. J. Electr. Power Energy Syst.*, vol. 43, no. 1, pp. 1114–1126, Dec. 2012, doi: 10.1016/j.ijepes.2012.06.045.

[14] P. Karuppanan and K. K. Mahapatra, "Active harmonic current compensation to enhance power quality," *Int. J. Electr. Power Energy Syst.*, vol. 62, pp. 144–151, Nov. 2014, doi: 10.1016/j.ijepes.2014.04.018.

[15] A. Boussaid, A. L. Nemmour, and A. Khezzar, "A novel strategy for shunt active filter control," *Electr. Power Syst. Res.*, vol. 123, pp. 154–163, Jun. 2015, doi: 10.1016/j.epsr.2015.02.008.

[16] A. Bhattacharya, C. Chakraborty, and S. Bhattacharya, "Shunt compensation," *IEEE Ind. Electron. Mag.*, vol. 3, no. 3, pp. 38–49, Sep. 2009, doi: 10.1109/MIE.2009.933881.
[17] R. Kumar, P. Chaturvedi, H. O. Bansal, and P. K. Ajmera, "Adaptive artificial neural network based control strategy for shunt active power filter," in *Proc. Int. Conf. Electr. Power Energy Syst. (ICEPES)*, 2016, pp. 194–199.
[18] F. Cupertino, M. Marinelli, P. Zanchetta, and M. Sumner, "Modelling and design of shunt active power filters using genetic algorithms," in *Proc. Eur. Conf. Power Electron. Appl.*, 2005, pp. 5–9.
[19] R. Kumar and H. O. Bansal, "Shunt active power filter: Current status of control techniques and its integration to renewable energy sources," *Sustain. Cities Soc.*, vol. 42, pp. 574–592, Oct. 2018, doi: 10.1016/j.scs.2018.07.002.
[20] J. Zhou, Y. Yuan, and H. Dong, "Adaptive DC-link voltage control for shunt active power filters based on model predictive control," *IEEE Access*, vol. 8, pp. 208348–208357, 2020, doi: 10.1109/ACCESS.2020.3038459.
[21] X. Nie and J. Liu, "Current reference control for shunt active power filters under unbalanced and distorted supply voltage conditions," *IEEE Access*, vol. 7, pp. 177048–177055, 2019, doi: 10.1109/ACCESS.2019.2957946.
[22] J. Kennedy and R. Eberhart, "Particle swarm optimization," in *Proc. IEEE Int. Conf. Neural Netw.*, Nov./Dec. 1995, pp. 1942–1948.
[23] R. N. Ray, D. Chatterjee, and S. K. Goswami, "A PSO based optimal switching technique for voltage harmonic reduction of multilevel inverter," *Expert Syst. Appl.*, vol. 37, no. 12, pp. 7796–7801, Dec. 2010, doi: 10.1016/j.eswa.2010.04.060.
[24] S. S. Patnaik and A. K. Panda, "Real-time performance analysis and comparison of various control schemes for particle swarm optimization-based shunt active power filters," *Int. J. Electr. Power Energy Syst.*, vol. 52, pp. 185–197, Nov. 2013.
[25] H. Karimi, M. Karimi-Ghartemani, M. R. Iravani, and A. R. Bakhshai, "An adaptive filter for synchronous extraction of harmonics and distortions," *IEEE Trans. Power Del.*, vol. 18, no. 4, pp. 1350–1356, Oct. 2003.
[26] R. Kumar and H. O. Bansal, "Hardware in the loop implementation of wavelet based strategy in shunt active power filter to mitigate power quality issues," *Electr. Power Syst. Res.*, vol. 169, pp. 92–104, Apr. 2019, doi: 10.1016/j.epsr.2019.01.001.
[27] H. Bansal, R. Sharma, and P. Shreeraman, "PID controller tuning techniques: A review," *J. Control Eng. Technol.*, vol. 2, no. 4, pp. 168–176, 2012.
[28] N. Babu, J. M. Guerrero, P. Siano, R. Peesapati, and G. Panda, "An improved adaptive control strategy in grid-tied PV system with active power filter for power quality enhancement," *IEEE Syst. J.*, vol. 15, no. 2, pp. 2859–2870, Jun. 2021, doi: 10.1109/JSYST.2020.2985164.
[29] A. Kumar and P. Kumar, "Power quality improvement for grid-connected PV system based on distribution static compensator with fuzzy logic controller and UVT/ADALINE-based least mean square controller," *J. Mod. Power Syst. Clean Energy*, vol. 9, no. 6, pp. 1289–1299, 2021, doi: 10.35833/MPCE.2021.000285.
[30] M. A. Mansor, K. Hasan, M. M. Othman, S. Z. B. M. Noor, and I. Musirin, "Construction and performance investigation of three-phase solar PV and battery energy storage system integrated UPQC," *IEEE Access*, vol. 8, pp. 103511–103538, 2020, doi: 10.1109/ACCESS.2020.2997056.
[31] C. M. N. Mukundan, P. Jayaprakash, U. Subramaniam, and D. J. Almakhles, "Binary hybrid multilevel inverter-based grid integrated solar energy conversion system with damped SOGI control," *IEEE Access*, vol. 8, pp. 37214–37228, 2020, doi: 10.1109/ACCESS.2020.2974773.
[32] S. Devassy and B. Singh, "Implementation of solar photovoltaic system with universal active filtering capability," *IEEE Trans. Ind. Appl.*, vol. 55, no. 4, pp. 3926–3934, Jul. 2019, doi: 10.1109/TIA.2019.2906297.
[33] A. Mishra, S. Chauhan, P. Karuppanan, and M. Suryavanshi, "PV based shunt active harmonic filter for power quality improvement," in *Proc. Int. Conf. Comput., Commun., Intell. Syst. (ICCCIS)*, Feb. 2021, pp. 905–910, doi: 10.1109/ICCCIS51004.2021.9397214.
[34] R. Kumar, "Fuzzy particle swarm optimization control algorithm implementation in photovoltaic integrated shunt active power filter for power quality improvement using hardware-in-the-loop," *Sustain. Energy Technol. Assessments*, vol. 50, Mar. 2022, Art. no. 101820, doi: 10.1016/j.seta.2021.101820.
[35] R. D. Patidar and S. P. Singh, "Digital signal processor based shunt active filter controller for customer-generated harmonics and reactive power compensation," *Electr. Power Compon. Syst.*, vol. 38, no. 8, pp. 937–959, May 2010, doi: 10.1080/15325000903571558.
[36] H. L. Jou, J. C. Wu, Y. J. Chang, Y. T. Feng, and W. P. Hsu, "New active power filter and control method," *IEE Proc.-Electr. Power Appl.*, vol. 152, no. 2, pp. 175–181, Mar. 2005. [Online]. Available: https://digital-library.theiet.org/content/journals/10.1049/ip-epa_20055120, doi: 10.1049/ip-epa:20055120.
[37] W. Liu, I.-Y. Chung, L. Liu, S. Leng, and D. A. Cartes, "Real-time particle swarm optimization based current harmonic cancellation," *Eng. Appl. Artif. Intell.*, vol. 24, no. 1, pp. 132–141, Feb. 2011, doi: 10.1016/j.engappai.2010.08.004.
[38] R. Kaushik, O. P. Mahela, P. K. Bhatt, B. Khan, S. Padmanaban, and F. Blaabjerg, "A hybrid algorithm for recognition of power quality disturbances," *IEEE Access*, vol. 8, pp. 229184–229200, 2020, doi: 10.1109/ACCESS.2020.3046425.
[39] N. Iqbal, A. Zerguine, and N. Al-Dhahir, "Decision feedback equalization using particle swarm optimization," *Signal Process.*, vol. 108, pp. 1–12, Mar. 2015, doi: 10.1016/j.sigpro.2014.07.030.
[40] K. Ai-Haddad, B. Singh, and A. Chandra, *Power Quality: Problems and Mitigation Techniques*. Hoboken, NJ, USA: Wiley, 2014.
[41] S. Mobin, E. Hiraki, H. Takano, and M. Nakaoka, "Simulation method for DSP-controlled active PFC high-frequency power converters," *IEE Proc.-Electr. Power Appl.*, vol. 147, no. 3, pp. 159–166, 2000.
[42] R. Kumar, H. O. Bansal, and D. Kumar, "Improving power quality and load profile using PV-battery-SAPF system with metaheuristic tuning and its HIL validation," *Int. Trans. Electr. Energy Syst.*, vol. 30, no. 5, pp. 1–19, May 2020, doi: 10.1002/2050-7038.12335.
[43] T. Eswaran and V. S. Kumar, "Particle swarm optimization (PSO)-based tuning technique for PI controller for management of a distributed static synchronous compensator (DSTATCOM) for improved dynamic response and power quality," *J. Appl. Res. Technol.*, vol. 15, no. 2, pp. 173–189, Apr. 2017, doi: 10.1016/j.jart.2017.01.011.
[44] *IEEE Recommended Practice for Powering and Grounding Sensitive Electronic Equipment*, Standard 1100-1992, Dec. 1992, pp. 1–256. [Online]. Available: https://ieeexplore.ieee.org/document/223448, doi: 10.1109/IEEESTD.1992.114798.10.1109/IEEESTD.1992.114798.
[45] T. S. Key and J.-S. Lai, "Costs and benefits of harmonic current reduction for switch-mode power supplies in a commercial office building," *IEEE Trans. Ind. Appl.*, vol. 32, no. 5, pp. 1017–1025, Sep./Oct. 1996, doi: 10.1109/28.536860.
[46] R. Kumar and H. O. Bansal, "Real-time implementation of adaptive PV-integrated SAPF to enhance power quality," *Int. Trans. Elect. Energy Syst.*, vol. 29, no. 5, p. e12004, 2019, doi: 10.1002/2050-7038.12004.